Materials Today Bio 14 (2022) 100233

Contents lists available at ScienceDirect

Materials Today Bio

journal homepage: www.journals.elsevier.com/materials-today-bio

Effect of naturally derived surgical hemostatic materials on the proliferation of A549 human lung adenocarcinoma cells

Wei-Dong Lü [a,*,1], Yi-Zhi Liu [b,1], Yan-Qi Yang [c], Zhi-Gang Liu [a], Kun Zhao [a], Jian-Rong Lu [d], Guang-Yan Lei [a], Yi-Yu Wang [d], Lin Cai [d], Rui-Fang Sun [c,**]

[a] Department of Thoracic Surgery, Tumor Hospital of Shaanxi Province, Affiliated to the Medical College of Xi'an Jiaotong University, Xi'an, Shaanxi, 710061, China
[b] Department of Medical Oncology, Tumor Hospital of Shaanxi Province, Affiliated to the Medical College of Xi'an Jiaotong University, Xi'an, Shaanxi, 710061, China
[c] Department of Pathology, School of Basic Medical Sciences, Xi'an Jiaotong University, Xi'an, Shaanxi, 710061, China
[d] Department of Pathology, Tumor Hospital of Shaanxi Province, Affiliated to the Medical College of Xi'an Jiaotong University, Xi'an, Shaanxi, 710061, China

ARTICLE INFO

Keywords:
Hemostatic materials
Gelatin sponge (GS)
Surgicel
Macrophage
Lymphocyte reaction

ABSTRACT

Hemostatic materials are generally applied in surgical operations for cancer, but their effects on the growth and recurrence of tumors are unclear. Herein, three commonly used naturally derived hemostatic materials, gelatin sponge, Surgicel (oxidized regenerated cellulose), and biopaper (mixture of sodium hyaluronate and carboxymethyl chitosan), were cocultured with A549 human lung adenocarcinoma cells *in vitro*. Furthermore, the performance of hemostatic materials and the tumorigenicity of the materials with A549 cells were observed after subcutaneous implantation into BALB/c mice. The *in vitro* results showed that biopaper was dissolved quickly, with the highest cell numbers at 2 and 4 days of culture. Gelatin sponges retained their structure and elicited the least cell infiltration during the 2- to 10-day culture. Surgicel partially dissolved and supported cell growth over time. The *in vivo* results showed that biopaper degraded rapidly and elicited an acute Th1 lymphocyte reaction at 3 days after implantation, which was decreased at 7 days after implantation. The gelatin sponge resisted degradation and evoked a hybrid M1/M2 macrophage reaction at 7–21 days after implantation, and a protumor M2d subset was confirmed. Surgicel resisted early degradation and caused obvious antitumor M2a macrophage reactions. Mice subjected to subcutaneous implantation of A549 cells and hemostatic materials in the gelatin sponge group had the largest tumor volumes and the shortest overall survival (OS), while the Surgicel and the biopaper group had the smallest volumes and the longest OS. Therefore, although gelatin sponges exhibited cytotoxicity to A549 cells *in vitro*, they promoted the growth of A549 cells *in vivo*, which was related to chronic M2d macrophage reaction. Surgicel and biopaper inhibited A549 cell growth *in vivo*, which is associated with chronic M2a macrophage reaction or acute Th1 lymphocyte reaction.

1. Introduction

Local application of hemostatic materials in surgical operation can significantly reduce blood loss, keep the operation field clear, shorten the operation time, and lessen the indwelling time of the drainage tube after operation [1]. At present, the commonly used hemostatic materials in operation include gelatin sponges (GSs), chitosan, renewable cellulose, and polysaccharides, among others. GS is used mostly in the clinic because of its low price and easy applicability. The porous structure of GS can absorb 45 times more blood than its own volume, activate platelets,

Abbreviations: GS, gelatin sponge; ECM, extracellular matrix; DMEM, Dulbecco's modified Eagle's medium; FDA, fluorescein diacetate; CLEC7A, C-type lectin domain family 7 member A; TNFSF14, TNF superfamily member 14; SLAM, signaling lymphocytic activation molecule; VEGF-A, vascular endothelial growth factor A; TBX21, T-box transcription factor 21; GATA3, GATA binding protein 3; TNF-α, tumor necrosis factor-α; ARG1, arginase-1; SDS–PAGE, sodium dodecyl sulfate–polyacrylamide gel electrophoresis; CCL1, C–C Motif Chemokine Ligand 1; CXCL8, C-X-C Motif Chemokine Ligand 8; Th, T helper cells; CTL, cytotoxic T lymphocyte cells; UBM, urinary bladder matrix; TAM, tumor-associated macrophage.

* Corresponding author. Department of Thoracic Surgery, Tumor Hospital of Shaanxi Province, Affiliated to the Medical College of Xi'an Jiaotong University, 309 Yanta West Road, Xi'an, Shaanxi, 710061, China.
** Corresponding author.
E-mail addresses: wdlu76@aliyun.com (W.-D. Lü), ruifang_sun@xjtu.edu.cn (R.-F. Sun).
[1] These authors contributed equally to this work.

https://doi.org/10.1016/j.mtbio.2022.100233
Received 14 January 2022; Received in revised form 28 February 2022; Accepted 2 March 2022
Available online xxxx

promote clot formation and achieve rapid hemostasis [2]. The absorption time for GS was nearly one month [3]. Oxidized cellulose and oxidized regenerated cellulose are absorbent local hemostatic materials obtained from cotton fibers oxidized by nitric oxide [4], both of which have the same hemostatic mechanism. The combination of acidic carboxyl groups and Fe^{+} in hemoglobin forms brown viscous adhesives, which then block damaged capillaries to stop bleeding. Surgicel is a regenerated oxidized cellulose widely used in surgical hemostasis [5]. The absorption time depends on the amount of blood absorbed and the nature of local tissues. Generally, it lasts for 3–6 weeks, but it can be detected four months after abdominal surgery [6]. Chitosan is a special alkaline polysaccharide that is the primary derivative of deacetylation of chitin [7]. It mainly achieves hemostasis by promoting erythrocyte aggregation and platelet adhesion and aggregation in blood. Chitosan-based hemostatic agents have great hemostatic and antibacterial properties [7,8].

Hemostatic materials are often used during the surgical resection of tumors. Previous studies have focused on their hemostatic effect, histocompatibility and antibacterial activity [9,10], but the effect of these hemostatic materials on tumor cells has not been reported in the literature. Three-dimensional (3D) scaffolds were successfully used to mimic the tumor microenvironment, and tumor cells cultured on the 3D scaffolds displayed better invasion ability [11–13]. There is the possibility that a few exfoliated tumor cells remain after surgery. If these hemostatic materials accelerate the growth of residual tumor cells on these 3D scaffolds, it is possible that they promote short-term recurrence of tumors. However, the implantation of extracellular matrix (ECM)-based scaffolds has been found to inhibit tumor formation [14–16]. Thus, whether hemostatic materials promote or resist tumor growth should be further clarified.

Naturally derived materials elicit different responses from tissues over time and based on their material properties when implanted *in vivo* [17]. Foreign body reactions against implanted materials includes five stages: initial protein adhesion, acute lymphocyte inflammation at the early phase, macrophage-associated chronic inflammation, foreign-body giant-cell reaction and fibrotic response [18–20]. The fast degradation of materials elicits acute inflammation, which will resolve without continuous material stimulation. However, the delayed degradation of these foreign materials will induce chronic macrophage and foreign body giant cell reactions, with the formation of fibrous encapsulation [18]. The degradation products and accompanying host cell infiltration will also affect residual tumor cells after surgery. The acute and chronic inflammation elicited by biomaterials involves polymorphonuclear leukocytes, immature dendritic cells, lymphocytes, monocytes and macrophages [21]. In the modified procedure, immune cells, including lymphocytes and macrophages, play central roles. Traditionally, proinflammatory type 1 immunity is associated with a tumor-suppressive environment [22,23], and the pro-regenerative type 2 immune response is related to tumor-permissive characteristics [24,25]. Nevertheless, naturally derived biomaterials present a type 2 immune bias but show tumor inhibition performance [16,26,27]. The immunophenotypes of naturally derived hemostatic materials when implanted and their effects on tumor growth remain unclear.

In the present study, three commonly used naturally derived hemostatic materials, GS, Surgicel (oxidized regenerated cellulose) and biopaper (mixture of sodium hyaluronate and carboxymethyl chitosan), were used as 3D scaffolds for tumor cell culture to observe the growth and proliferation of tumor cells *in vitro*. Furthermore, the performance of hemostatic materials subcutaneously implanted into BALB/c mice and the related lymphocyte and macrophage phenotypes were observed. Moreover, the tumorigenicity of the hemostatic material when subcutaneously implanted along with a small number of tumor cells into mice was investigated. We hypothesized that the three hemostatic materials studied would present different performances when cocultured with tumor cells *in vitro* and implanted with tumor cells *in vivo*.

2. Materials and methods

2.1. Materials and material characterizations

Three commonly used hemostatic materials were studied, namely, GS (Jinling Pharmaceutical Co., Ltd. Nanjing, Jiangsu, China), Surgicel (Ethicon, INC., Somerville, NJ, USA) and biopaper (Datsing Bio-Tech Co., Ltd., Beijing, China). The hemostatic materials were gross examined and fixed in 4% paraformaldehyde for hematoxylin and eosin (H&E) staining as previously described [28]. The ultrastructure was investigated under a Nova NanoSEM 230 microscope (FEI Co., Hillsboro, OR, USA). Hemostatic materials contacted with fresh blood and the *in vitro* degradation test of the hemostatic materials were described in supplementary file 1 and supplementary file 2.

2.2. Cell culture

The *in vitro* cytotoxicity test of the hemostat material' extract was described in supplementary file 3. For the cell-material contact evaluation, samples were trimmed into 6-mm diameter rounds and incubated in 24-well plates at 37 °C in 200 μL of Dulbecco's modified Eagle's medium (DMEM) supplemented with 1% antibiotic-antimycotic solution and 10% fetal bovine serum for 10 min. Then, A549 human lung adenocarcinoma cells (ATCC, 1×10^5 cells) were added to each well and incubated at 37 °C with 5% CO_2 for 60 min. Finally, 1 mL of DMEM was added to the plates for further cell culture. The culture medium was replaced every other day. Cells cultured without hemostatic materials (2D culture) were used as controls (n = 12).

2.3. Cell seeding analysis and growth factor assay

Gross and light microscopy investigations were carried out using routine conditions. Fluorescein diacetate (FDA) staining was used to examine the light microscopy properties of each group after 10 days of culture (n = 3). FDA stains viable cells green, and the staining procedure has been previously described [29]. The three materials were retrieved after 2 days of culture and fixed in 2.5% glutaraldehyde for SEM investigation (n = 3). Since only GS and Surgicel were retained at 10 days of culture, the two materials were harvested for SEM examination (n = 3). The number of A549 cells at 2, 4, 6, 8 and 10 days of culture for each group (n = 9) was determined with the Alamar Blue assay [30]. Briefly, the medium in the plate was removed, and 2 mL of 5% Alamar Blue solution were added and incubated for 3 h. The fluorescent signal was measured with a fluorescence microplate reader (Spectrafluor, Tecan, Sunrise, Austria) at an excitation wavelength of 540 nm and an emission wavelength of 590 nm. A549 cells in graded number were subjected to the Alamar Blue assay to obtain a standard curve. The A549 cell number in each sample was calculated from the standard curve. In the Alamar Blue assay, the background fluorescence of undissolved GS or Surgicel was detected, and no background fluorescence was generated by the hemostats. This excluded the influence of the hemostats on detection reagents. Growth factor (IL-8, bFGF, and VEGF) levels in 10-day cultures (n = 9) were assayed with ELISA as previously described [29].

2.4. Performance of the hemostatic materials after subcutaneous implantation

2.4.1. Ethics statement

All animal procedures were performed in accordance with the Guidelines for Care and Use of Laboratory Animals of Xi'an Jiaotong University and approved by the Animal Ethics Committee of Xi'an Jiaotong University (No. 2021320).

2.4.2. Subcutaneous implantation of hemostatic materials

Before use, the three hemostatic materials were cut into squares (10 mm × 10 mm). After induction of anesthesia with 4% isoflurane and

maintenance of anesthesia with 2% isoflurane, a 10-mm incision in the right upper flanks of 6-week-old male BALB/c mice (provided by the Medical Laboratory Animal Center of Xi'an Jiaotong University) was cut for implantation of the sample. Surgical staples were used to close the skin. Mice who did not undergo implantation (injection of normal saline) were used as controls (n = 24). Samples (hemostatic materials and surrounding tissues) were retrieved at 3, 7, 14 and 21 days after implantation. Some of the harvested samples were stored in liquid nitrogen for subsequent analysis. The other samples were fixed in 4% paraformaldehyde for 24 h for paraffin sectioning.

2.4.3. Histology and immunofluorescence staining

Paraffin-embedded tissues were cut into 5-μm-thick sections and stained with H&E. Masson's trichrome technique was used to examine collagen fibers. T cells were detected by immunofluorescence staining with CD3 monoclonal antibody (dilution 1:100, Abcam, Cambridge, UK). Macrophages were tested with rabbit anti-mouse F4/80 monoclonal antibody (dilution 1:200, Abcam). T cell subtypes were distinguished by double immunofluorescence staining with rat anti-mouse CD4 monoclonal antibody (dilution 1:400, Abcam) and rabbit anti-mouse CD8-α monoclonal antibody (dilution 1:1000, Abcam). Macrophage M1/M2 subtypes were investigated by double staining with rat anti-mouse CD86 (dilution 1:200, Cell Signaling Technology Inc., Danvers, MA, USA) and rabbit anti-mouse CD163 antibodies (dilution 1:500, Cell Signaling Technology). Macrophage M2a and M2b subsets were investigated by double staining with rat anti-mouse C-type lectin domain family 7 member A (CLEC7A, M2a marker) monoclonal antibody (dilution 1:50, Invitrogen, Thermo Fisher Scientific, Carlsbad, CA, USA) and rabbit anti-TNF superfamily member 14 (TNFSF14, M2b marker) polyclonal antibody (dilution 1:200, Invitrogen). Macrophage M2a and M2c subsets were distinguished by double staining with rat anti-CLEC7A antibody (dilution 1:50, Invitrogen) and rabbit anti-signaling lymphocytic activation molecule (SLAM, M2c marker) polyclonal antibodies (dilution 1:200, Invitrogen). The macrophage M2d subset was detected by double immunofluorescence staining with rat anti-F4/80 monoclonal antibody (dilution 1:50, Invitrogen) and rabbit anti-vascular endothelial growth factor A (VEGF-A) polyclonal antibody (dilution 1:200, Invitrogen). Secondary antibodies, including Alexa Fluor 555-labeled donkey anti-rat IgG and Alexa Fluor 488-labeled goat anti-rabbit IgG, were obtained from Abcam. DAPI was used to stain cell nuclei. The immunofluorescence staining procedure has been described previously [11].

2.4.4. Quantitative real-time polymerase chain reaction (qRT–PCR)

The harvested subcutaneous samples were homogenized in liquid nitrogen, and RNA was isolated using TRIzol reagent (Invitrogen). The PCR primers used were listed in Table 1. A LightCycler 96 System (Roche, Basel, Switzerland) was used to conduct the PCR analysis. The PCR conditions started with preheating at 95 °C for 5 min, followed by 40 cycles of 15 s at 95 °C, annealing at 56 °C for 30 s and extension at 72 °C for 1 min. T-box transcription factor 21 (TBX21), GATA binding protein 3 (GATA3), tumor necrosis factor-α (TNF-α) and arginase-1 (ARG1) gene expression (n = 6) was normalized to GAPDH. Gene expression ratios of GATA3/TBX21 and ARG1/TNF-α were used to quantify T helper cell and macrophage polarization, respectively [31].

Table 1
Primers for quantitative RT-PCR.

Gene	Sequence
TBX21	Forward 5′- CAGACAGAGATGATCATCACCA-3′
	Reverse 5′- CAGTAAATGACAGGAATGGGA-3′
GATA3	Forward 5′- GAAGGCATCCAGACCCGAAAC-3′
	Reverse 5′- ACCCATGGCGGTGACCATGC-3′
TNF-α	Forward 5′-AAGCCTGTAGCCCACGTCGTA-3′
	Reverse 5′-GGCACCACTAGTTGGTTGTCTTTG-3′
ARG1	Forward 5′-GAACACGGCAGTGGCTTTAAC-3′
	Reverse 5′-TGCTTAGTTCTGTCTGCTTTGC-3′
GAPDH	Forward 5′-CTGGCATTGGGTCTACTGCT-3′
	Reverse 5′-GTCTACCCAATTGCCCCACT-3′

2.4.5. Western blot analysis

Protein from the harvested samples was extracted with the Proteo-Prep® Total Extraction Sample Kit (Sigma–Aldrich, St Louis, MO, USA). Protein concentration was detected by a bicinchoninic acid (BCA) kit (Beyotime, Jiangsu, China). A 20-μg sample of extracted protein was separated by sodium dodecyl sulfate–polyacrylamide gel electrophoresis (SDS–PAGE) and transferred to PVDF membranes (Millipore, Darmstadt, Germany). The membrane was further blocked with 5% nonfat milk and incubated overnight at 4 °C with primary antibodies against TBX21, GATA3, TNF-α, ARG1, CLEC7A, C–C Motif Chemokine Ligand 1 (CCL1, M2b marker), SLAM, C-X-C Motif Chemokine Ligand 8 (CXCL8, M2d marker) and β-actin (all dilutions 1:1,000, Invitrogen). Then, the membrane was incubated with horseradish peroxidase-conjugated goat secondary antibodies (Invitrogen). The protein band (n = 6) was visualized using an enhanced chemiluminescence system (GE Healthcare Life Sciences), and densitometric quantification was conducted with the ImageJ system (National Institutes of Health, Bethesda, MD, USA). Protein values were normalized to β-actin.

2.5. Subcutaneous tumorigenesis of A549 cells and hemostatic materials

Anesthesia was induced and maintained with 4% and 2% isoflurane. After a 10-mm incision was made in the right upper flanks of 6-week-old male BALB/c mice, 200 μL of A549 human lung adenocarcinoma cells (concentration 5×10^5 cells/mL) was injected into the surface of the muscle. Then, the hemostatic material (10 mm × 10 mm) was implanted in contact with the muscle and A549 cells. Mice that did not undergo hemostatic material implantation were used as controls (n = 23). A total of 3, 3, 3 and 6 mice were sacrificed at 3-, 7-, 14- and 21-days post-implantation, and tumors were harvested for further investigation. The remaining 8 mice were retained for survival observation.

Tumor volumes were measured as previously described [29]. The harvested tumors were stored in liquid nitrogen for western blot analysis or fixed in 4% paraformaldehyde for paraffin sectioning. Histological and immunofluorescence staining were performed as described in the section describing the subcutaneous implantation of hemostatic materials.

2.6. Statistical analysis

All statistical analyses were carried out using IBM SPSS Statistics (version 25.0, IBM Corp., Armonk, NY, USA). Data are expressed as the mean ± standard deviation (SD). Statistical comparisons were conducted with ANOVA followed by Tukey's test for multiple comparisons. Kaplan–Meier estimates of overall survival (OS) were computed by the log-rank test. A value of $p < 0.05$ was considered statistically significant.

3. Results

3.1. Gross, ultrastructural and histological images showed different pore structures

Fig. 1A shows that all three hemostatic materials were white and porous, but GS was thick, and biopaper was dense and smooth on the surface. The SEM micrographs shown in Fig. 1B depict the porous structure of GS and biopaper, but the pore wall of the biopaper was thinner than that of GS. For Surgicel, the parallel fibrils were aggregated and formed columnar fibers. Fig. 1C illustrates the irregular arrangement of fibers with pores of varying sizes in GS, the flaky distributed fiber-like structures in Surgicel, and the microfibers with micropores in biopaper.

3.2. Cell seeding presented cytotoxicity of gelatin sponge and surgicel

Gross examination of the A549 cells seeded at 10 days of culture, as

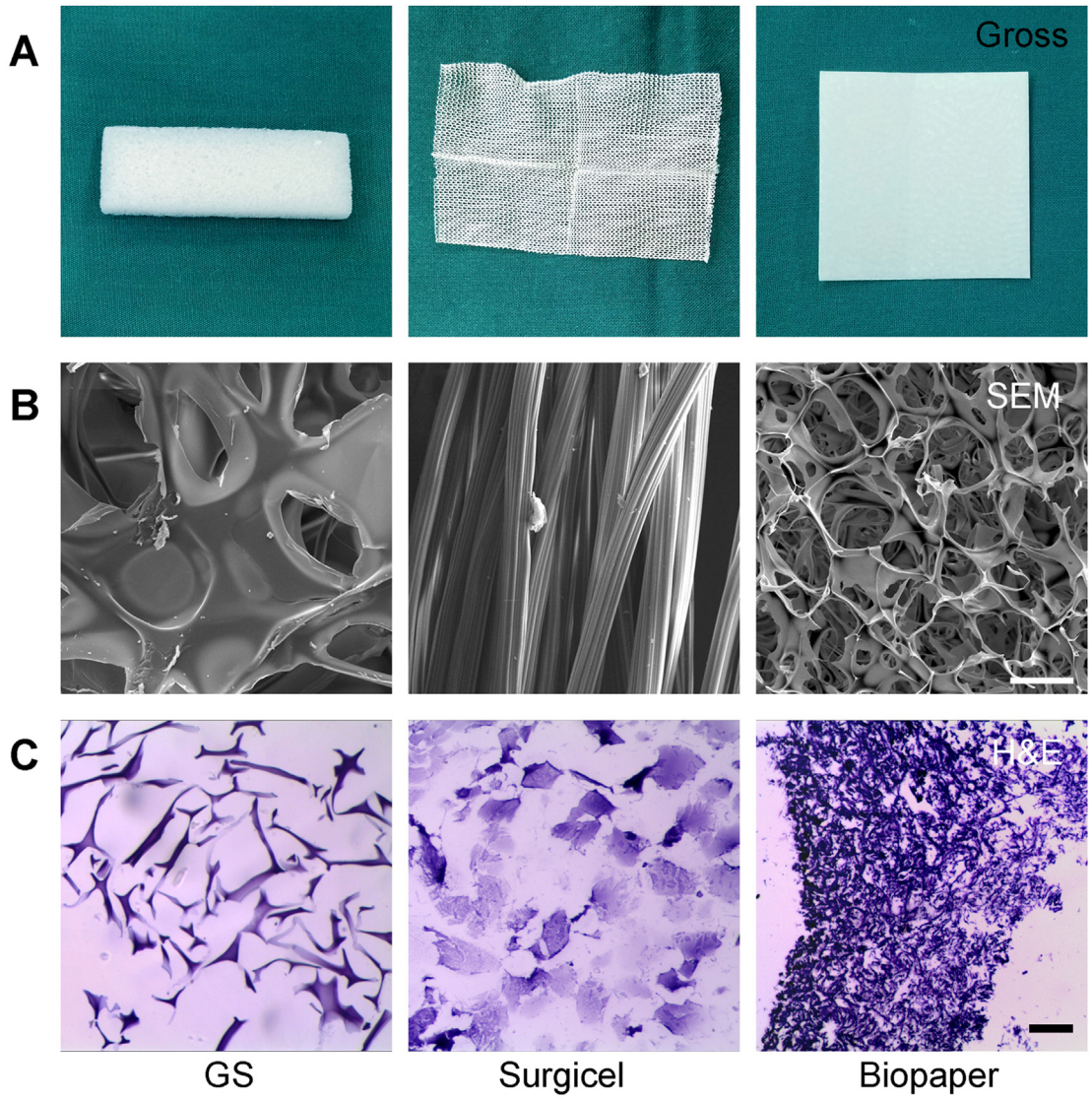

Fig. 1. Representative gross appearance (A), SEM investigation (B) and H&E staining (C) of gelatin sponge (GS), Surgicel and biopaper (scale bar for SEM = 50 μm; scale bar for H&E = 100 μm).

shown in Fig. 2A, revealed that the structure of GS was retained, while that of Surgicel was partially dissolved. No residue was found for the biopaper group. The live cell staining shown in Fig. 2B indicates that the biopaper group had a similar cell distribution and shape to the control group at 10 days of culture. The Surgicel group had fewer cells and a higher proportion of negative cells, and the GS group had few living cells after 10 days of culture. SEM in Fig. 2C illustrated that GS and Surgicel retained their structure and A549 cell attachments after 2 days of culture. The biopaper presented a gel-like structure, and the A549 cells infiltrated into the gels. The biopaper had dissolved and formed a gel-like structure during the first several minutes, while GS and Surgicel did not, which was confirmed by the hemostatic materials in contact with fresh blood presented in Figure S1. When the culture medium was replaced, the gel-like structure was completely dissolved and discarded. At 10 days of culture, only a few cells were found on the surface of GS. The columnar fibers of Surgicel had rough surfaces with visible cell clusters, implying that the structure changed with time and increased cell growth.

Fig. 2D shows that the cell numbers of the control group, the Surgicel group, and the biopaper group increased with time, but the cell numbers of the GS group decreased with time. The GS group had similar cell numbers per well as the Surgicel group at 2 days of culture, but the GS group had the lowest cell number per well at 4, 6, 8 and 10 days of culture. The biopaper group had the highest cell number per well at 2 and 4 days of culture and had comparable cell numbers per well to the control group at 6, 8 and 10 days of culture ($p = 0.058$, 0.463 and 0.542). The cell numbers in the Surgicel group at 4, 6, 8 and 10 days of culture were lower than those in the control group and the biopaper group (all $p < 0.001$), but higher than those in the GS group (all $p < 0.001$).

Fig. 2E shows the assays of the growth factors IL-8, bFGF, and VEGF in A549 cells cultured with hemostatic materials for 10 days. The biopaper group had higher levels of IL-8 ($p = 0.013$) but similar levels of bFGF and VEGF secretion ($p = 0.054$ and 0.287) compared with the control group. The biopaper group and the control group had more IL-8, bFGF, and VEGF secretion than the GS group and the Surgicel group (all $p < 0.001$). The Surgicel group had more IL-8, bFGF, and VEGF secretion than the GS group (all $p < 0.001$).

Figure S2A shows the three hemostatic materials were extracted with MEM, and biopaper completely dissolved after extraction. Figure S2B presents the control, the Surgicel and the biopaper group had similar cell morphology compare to the blank control. Cell deform and shrink were found in the phenol positive control and the GS group, implying cytotoxicity of the extract of GS. Figure S2C shows light color for the phenol positive control and the GS group, especially for the phenol group. Figure S2D shows similar cell viability values in the control, the Surgicel

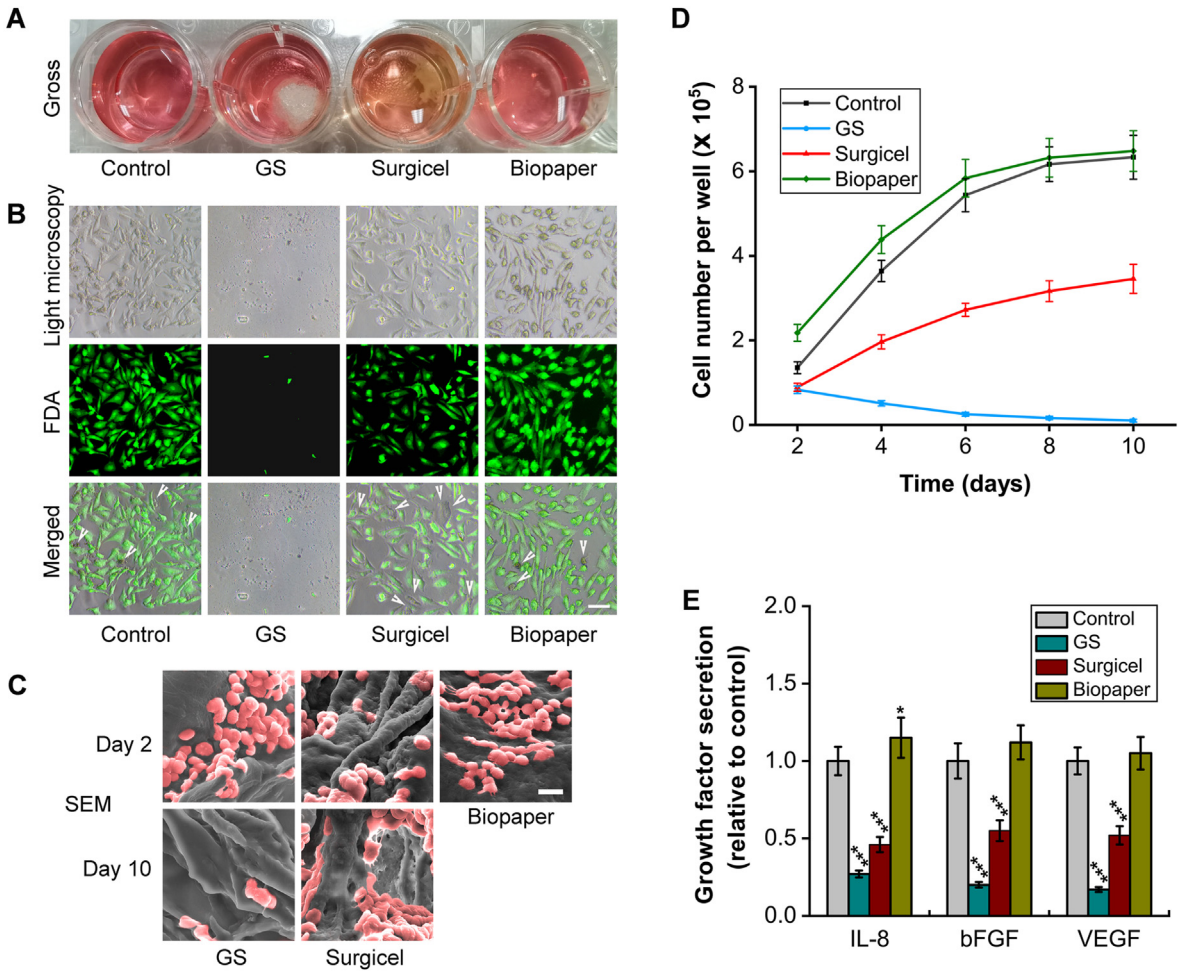

Fig. 2. Cell repopulation patterns and growth factor assays for A549 cells cultured with hemostatic materials. (A) Representative gross appearance at 10-day culture. (B) Representative light microscopic investigation, fluorescein diacetate (FDA) staining of living cells and their merged images at 10 days of culture (scale bar = 50 μm). The arrows show the negative staining cells. (C) Representative SEM examination of A549 cells seeded on hemostatic materials at 2 and 10 days of culture (scale bar = 10 μm). (D) Cell viability detection at different time points. (E) Growth factor (IL-8, bFGF, and VEGF) assays at 10 days of culture. Data are presented as the mean ± SD (*$p < 0.05$, ***$p < 0.001$).

and the biopaper group, while the cell viability values of the phenol group and the GS group were less than those of the control group ($p < 0.001$ and $p = 0.003$), implying the cytotoxicity of the two groups.

3.3. Subcutaneous implantation of hemostatic materials showed different tissue responses and immunophenotypes at acute and chronic inflammatory phases

3.3.1. Hemostatic materials underwent host cell repopulation and collagen deposition

The three hemostatic materials have different performances in mouse subcutaneous implantation. Biopaper was dissolved several minutes after implantation. The volumes of GS and Surgicel decreased with time, especially for Surgicel (Figure S3A). The thickness of undegraded hemostatic materials measured with light microscope in Figure S3B presented similar thickness for the GS and the Surgicel group at 3 and 7 days after implantation, but the Surgicel group had less thickness than the GS group at 14 and 21 days after implantation ($p = 0.015$ and $p < 0.001$). The degradation pattern is consistent to the *in vitro* degradation performance of hemostatic materials showed in Figure S4 and described in Supplementary file 2.

GS and Surgicel retained their structures at 3 days after implantation, with lymphocyte-like cells infiltrating the materials (Fig. 3A). At 7 days after implantation, GS was repopulated by host cells, with the formation of blue-stained collagen fibers (Fig. 3B). The host cells continuously infiltrated at 14 and 21 days after implantation, with an increase in collagen fiber thickness. Dense collagen deposition on the surface of GS formed fibrous encapsulation (Fig. 3B). For Surgicel at 7 days after implantation, the material spaces were occupied by thrombosis and ingrowth of host cells and collagen fibers (Fig. 3A and B). For Surgicel at 14 and 21 days after implantation, collagen fibers and host cells completely invaded and replaced the material structures. Biopaper was completely dissolved during the initial several minutes and evoked notable lymphocyte responses at 3 days after implantation (Fig. 3A). The lymphocyte responses decreased at 7 days after implantation. Subcutaneous tissues at 14 and 21-day retrieval presented normal cells and ECM structures.

3.3.2. The biopaper group presented Th1 lymphocyte responses at acute inflammatory phases

Immunofluorescence staining for T cells in Fig. 4A shows $CD3^+$ cells infiltrated into the pores of the material, and Fig. 4B shows that the biopaper group presented the largest number of cells at 3-day retrieval. The infiltrated lymphocytes in the biopaper group were mostly $CD4^+$ T cells (T helper cells, Th) and a few $CD8^+$ cells (cytotoxic T lymphocyte cells, CTL) (Fig. 4C), which induced tumor cell death. The lymphocyte response decreased at 7-day retrieval, as did the proportion of $CD4^+$ cells (Fig. 4D, $p < 0.001$). The GS group had more $CD3^+$ cells and a higher

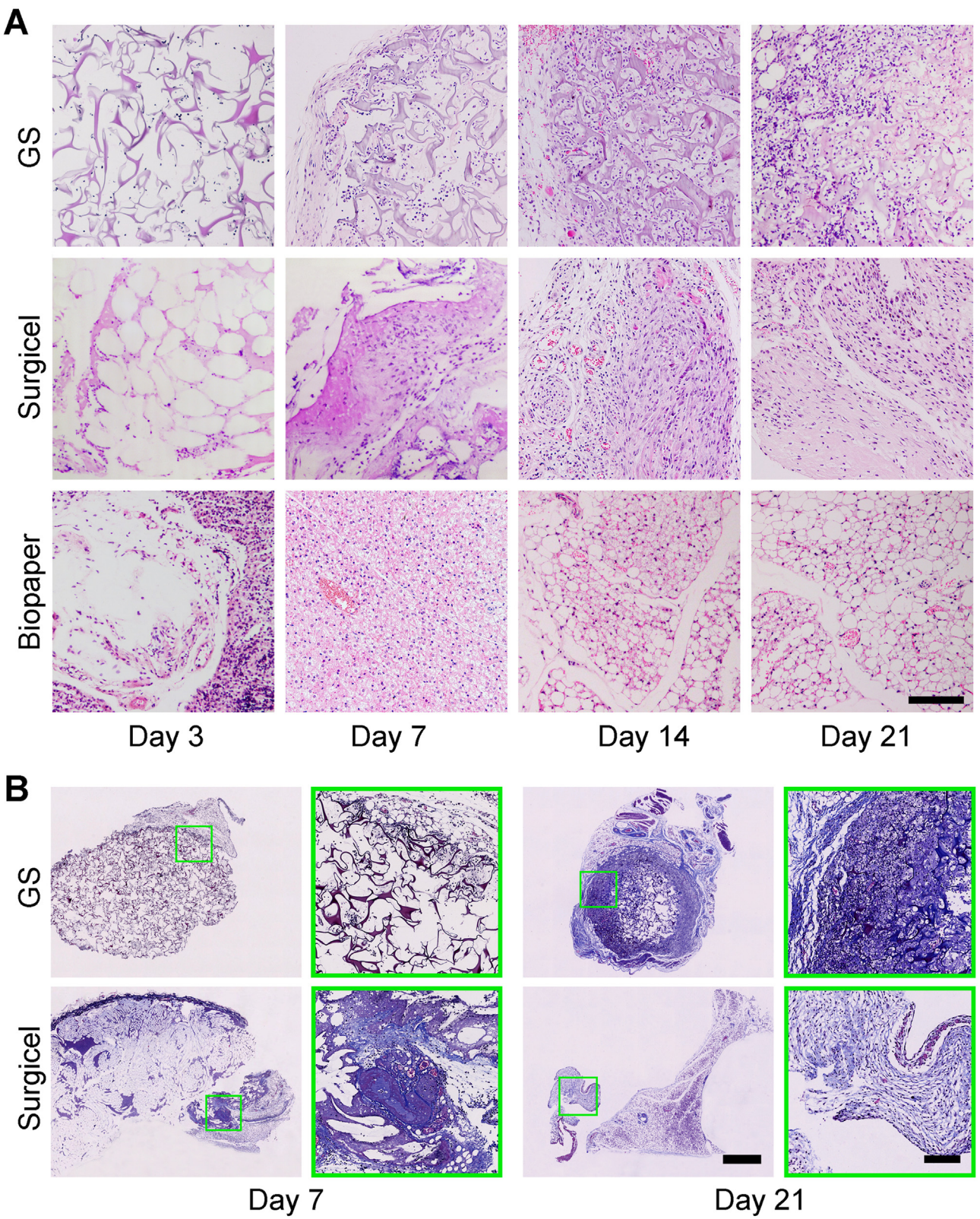

Fig. 3. Histological staining of subcutaneous implantation of hemostatic materials. (A) Representative H&E staining for GS, Surgicel and biopaper at 3, 7, 14 and 21 days after implantation (scale bar = 200 μm). (B) Masson's trichrome staining for GS and Surgicel at 7 and 21-day retrieval (scale bar = 1 mm for original images and scale bar = 200 μm for amplified images).

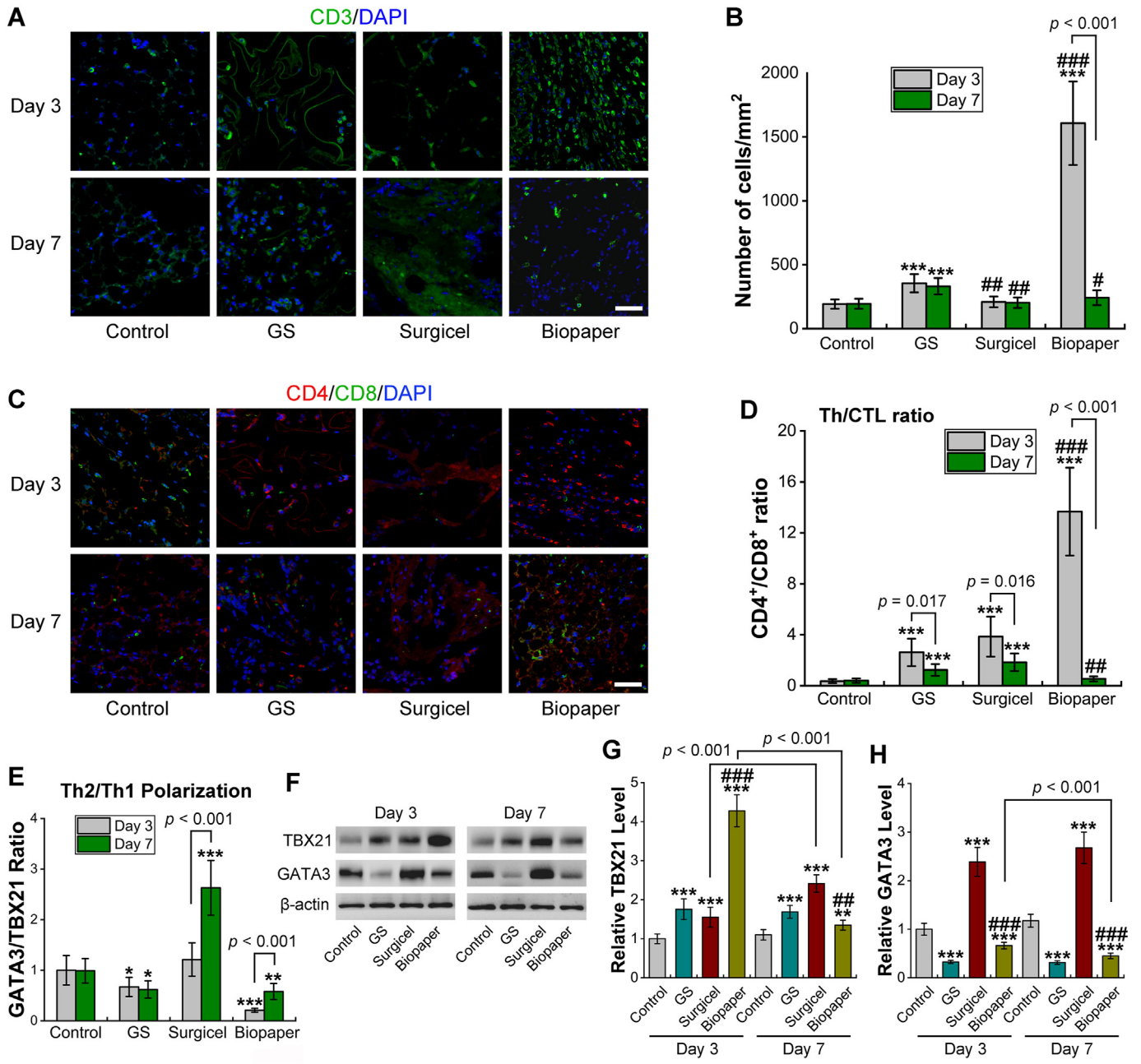

Fig. 4. The immunophenotypes of T cells for subcutaneous implantation of hemostatic materials at 3 and 7 days after implantation. (A) Representative immunofluorescence images of $CD3^+$ T cells (green) and nuclei (blue) (scale bar = 50 μm). (B) The T cell number comparison for the control, GS, Surgicel and biopaper groups. (C) Representative images of $CD4^+$ T cells (red), $CD8^+$ cells (green) and nuclei (blue) (scale bar = 50 μm). (D) The cell subtype ratio ($CD4^+$ cells/CD8+ cells) comparison for the four groups. (E) Relative GATA3 and TBX21 mRNA level ratios after subcutaneous implantation of hemostatic materials at 3 and 7-day retrieval as measured by qRT–PCR. (F) Representative immunoblot of TBX21, GATA3 and β-actin for the four groups at 3 and 7-day retrieval. (G) The relative protein band densitometric quantification of TBX21. (H) The relative protein band densitometric quantification for GATA3. Data are presented as the mean ± SD (*$p < 0.05$, **$p < 0.01$ and ***$p < 0.001$ versus the control group; #$p < 0.05$, ##$p < 0.01$ and ###$p < 0.001$ versus the GS group). (For interpretation of the references to colour in this figure legend, the reader is referred to the Web version of this article.)

proportion of $CD4^+$ cells at 3 and 7-day retrieval than the control and Surgicel groups (all $p < 0.001$). The Surgicel had less $CD3^+$ cells ($p = 0.001$ and 0.002), but had similar proportion of $CD4^+$ cells compared with the GS group at 3 and 7-day retrieval ($p = 0.142$ and 0.109).

The qRT–PCR results shown in Fig. 4E indicate that the ratio of GATA3/TBX21 (Th2/Th1 polarization) in the GS group was lower than that in the control group at 3 and 7-day retrieval ($p = 0.041$ and 0.012). The GATA3/TBX21 ratio in the Surgicel group was comparable to that in the control group at 3-day retrieval ($p = 0.269$), with the highest GATA3/TBX21 ratio for the Surgicel group being observed at 7-day retrieval. The biopaper group had the lowest GATA3/TBX21 ratio at 3-day retrieval and the ratio was increased at 7-day retrieval ($p < 0.001$). Western blot analysis results shown in Fig. 4F and G showed that the biopaper group expressed the highest TBX21 levels at 3-day retrieval, and the TBX21 levels were greatly decreased at 7-day retrieval ($p < 0.001$). The GS group and the Surgicel group had higher TBX21 levels than the control group at 3 and 7-day retrieval (all $p < 0.001$). Fig. 4F and H shows that, at 3 and 7-day retrieval, the Surgicel group had the highest GATA3 levels, and the GS group had the lowest GATA3 levels. The GATA3 levels in the biopaper group were higher than those in the GS group but lower than

those in the control and Surgicel groups at 3 and 7-day retrieval (all $p < 0.001$). In particular, the GATA3 levels were decreased at 7-day retrieval compared with those at 3-day retrieval ($p < 0.001$).

3.3.3. *Hemostatic materials showed different macrophage immunophenotypes at chronic inflammatory phases*

Immunofluorescence staining for macrophages shown in Fig. 5A and B showed that the biopaper group had similar numbers of F4/80+ macrophages compared with the control group at 7 and 21 days after implantation ($p = 0.617$ and 0.901). The Surgicel group and the GS group had similar numbers of macrophages at the two time points ($p = 0.762$ and 0.653). The latter two groups had more macrophages than the two former groups at 7 and 21 days after implantation ($p < 0.001$). For the nonmaterial control group, the infiltrated macrophages were confirmed to be predominantly of the M2 subtype (CD163+, Fig. 5C and D). The GS group had more M2 macrophages than M1 ($CD86^+$) macrophages, and the M2 macrophage proportion increased at 21 days after implantation compared with that at 7 days after implantation (76.3% versus 67.9%, $p = 0.023$). The Surgicel group had more M2 macrophages than M1 macrophages at 7 days after implantation, and the macrophage proportion of M2 and M1 macrophages at 21 days was similar to that at 7 days after implantation (78.7% versus 77.6%, $p = 0.796$). The biopaper group

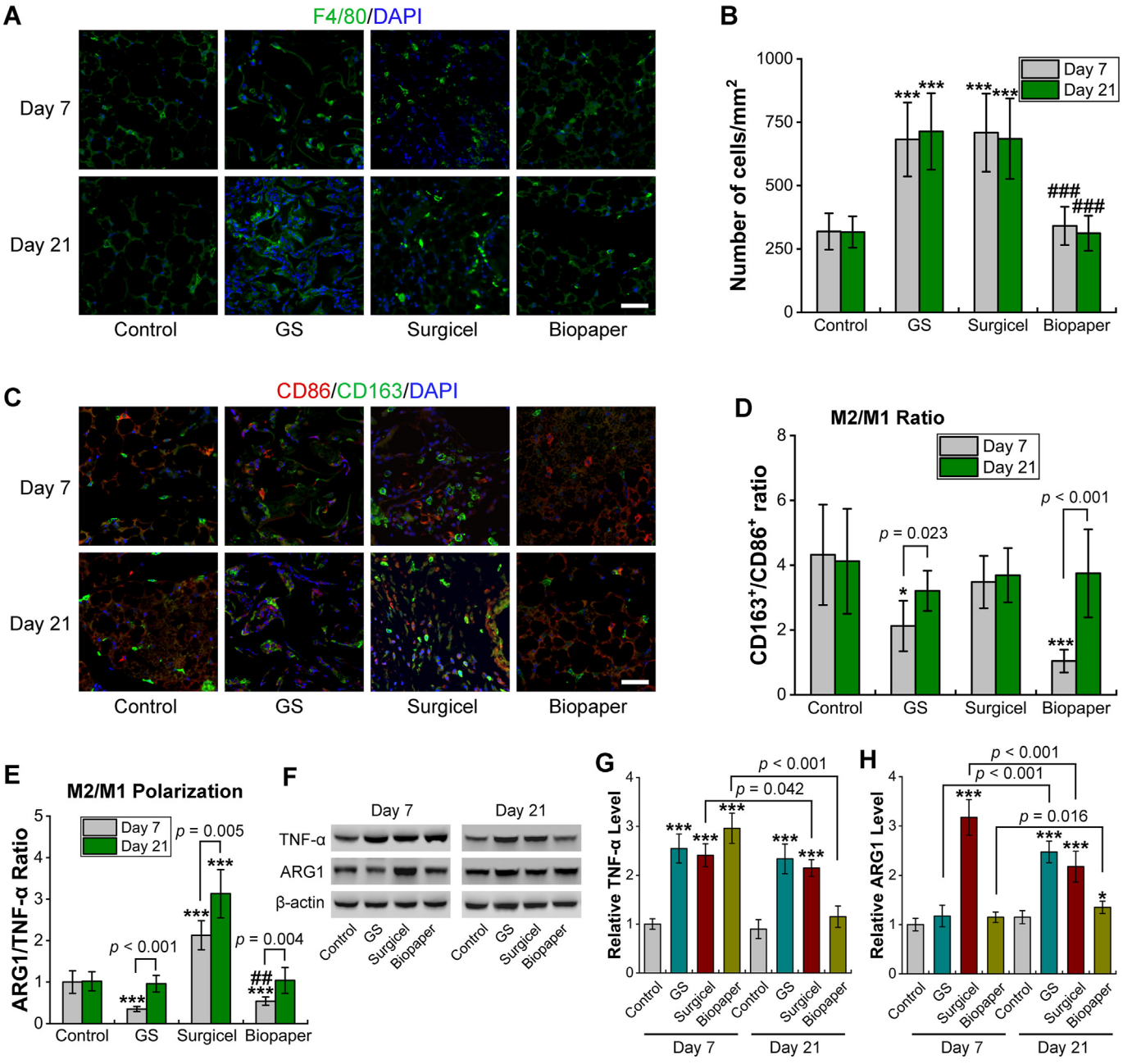

Fig. 5. The immunophenotypes of macrophages after subcutaneous implantation of hemostatic materials at 7 and 21-day retrieval. (A) Immunofluorescence images of F4/80+ cells (green) and nuclei (blue) (scale bar = 50 μm). (B) The macrophage number comparison for the control, GS, Surgicel and biopaper groups. (C) Immunofluorescence images of $CD86^+$ cells (red), CD163+ cells (green) and nuclei (blue) (scale bar = 50 μm). (D) The macrophage subtype ratio (C163+ cells/CD86+ cells) comparison for the four groups. (E) Relative arginase-1 (ARG1) and TNF-α mRNA level ratios at 7 and 21-day retrieval. (F) Representative immunoblot of TNF-α, ARG1 and β-actin at 7 and 21-day retrieval. (G) The relative protein band densitometric quantification of TNF-α. (H) The relative protein band densitometric quantification for ARG1. Data are presented as the mean ± SD (*$p < 0.05$ and ***$p < 0.001$ versus the control group; ##$p < 0.01$ and ###$p < 0.001$ versus the GS group). (For interpretation of the references to colour in this figure legend, the reader is referred to the Web version of this article.)

had comparable numbers of M2 and M1 macrophages at 7-day retrieval (50.9% versus 49.1%). At 21 days after implantation, the number of M1 macrophages were markedly decreased compared with that at 7 days after implantation (21.1% versus 49.1%, $p < 0.001$).

Fig. 5E shows that the GS group had the lowest ARG1/TNF-α ratio (M2/M1 polarization) at 7-day retrieval, and the ratio increased and was similar to that of the control group at 21-day retrieval ($p = 0.649$). The Surgicel group had a higher ARG1/TNF-α ratio than the control group at 7-day retrieval ($p < 0.001$) and had the highest ARG1/TNF-α ratio at 21-day retrieval. The biopaper group had the second lowest ARG1/TNF-α ratio at 7-day retrieval and had a comparable ratio to the control group at 21-day retrieval ($p = 0.902$). Western blot analysis results presented in Fig. 5F and G showed TNF-α levels of the GS group, the Surgicel group and the biopaper group were higher than the control group (all $p < 0.001$), and the biopaper group exhibited the highest TNF-α levels at 7 days after implantation. TNF-α levels were decreased in the Surgicel group and the Biopaper group at 21 days after implantation compared with those at 7 days after implantation ($p = 0.042$ and $p < 0.001$). Fig. 5F and H shows that the Surgicel group had the highest ARG1 levels at 7 days after implantation. The ARG1 levels increased in the GS group but

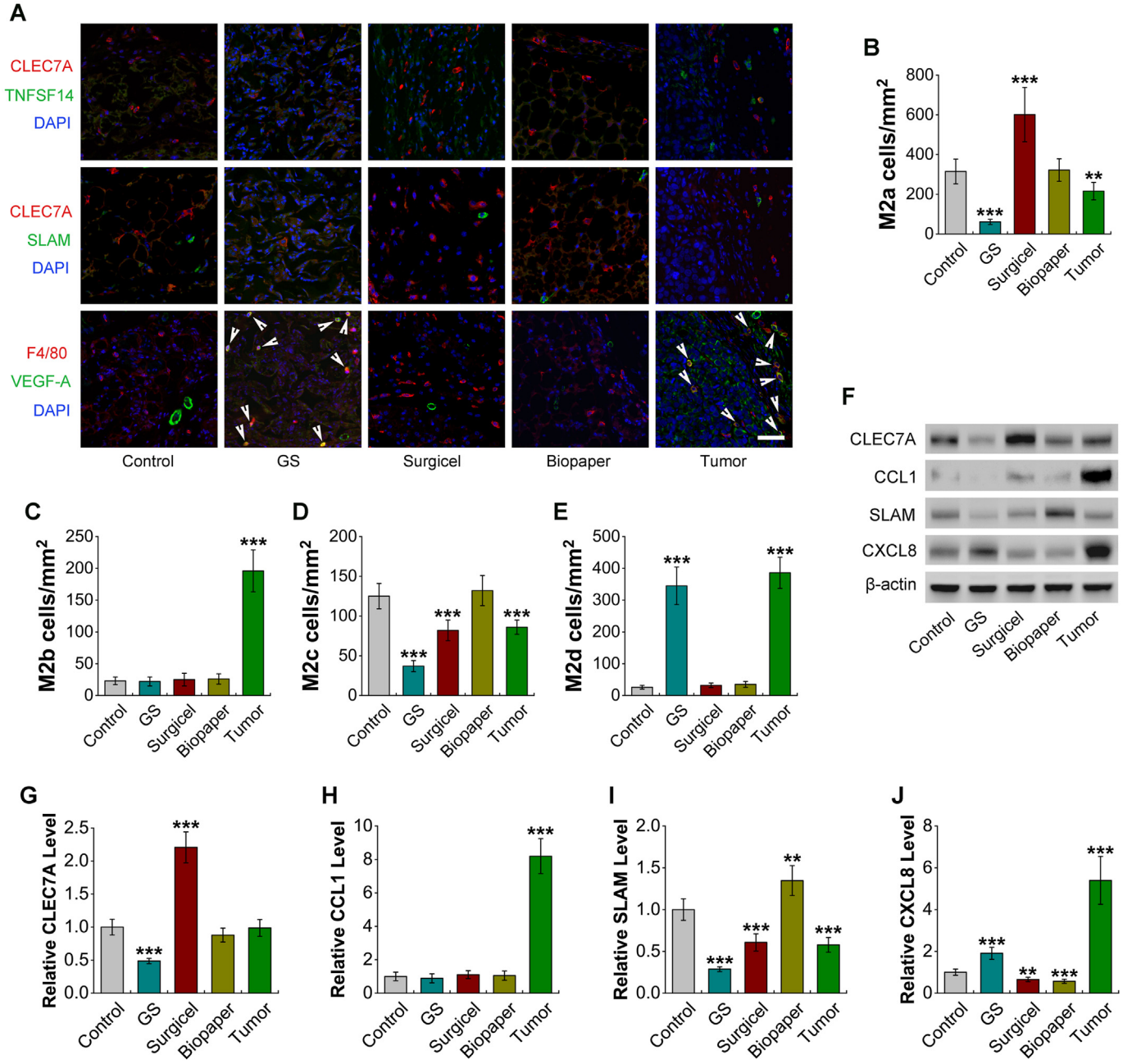

Fig. 6. The subtype immunophenotypes of M2 macrophages for subcutaneous implantation of hemostatic materials at 21-day retrieval. (A) Representative immunofluorescence images of C-type lectin domain family 7 member A (CLEC7A, red, M2a marker), TNF superfamily member 14 (TNFSF14, green, M2b marker), signaling lymphocytic activation molecule (SLAM, green, M2c marker), F4/80 (red), vascular endothelial growth factor A (VEGF-A, green, M2d marker) and nuclei (blue) for the control, GS, Surgicel and biopaper groups (scale bar = 50 μm). Note M2d macrophages were labeled with double F4/80 and VEGF-A positive staining (arrows). (B–E) The M2a-M2d macrophage number comparison for the four groups. (F) Representative immunoblot of CLEC7A, C–C Motif Chemokine Ligand 1 (CCL1, M2b marker), SLAM, C-X-C Motif Chemokine Ligand 8 (CXCL8, M2d marker) and β-actin at 21-day retrieval. (G–J) Relative protein band densitometric quantification. Data are presented as the mean ± SD (**$p < 0.01$, ***$p < 0.001$). (For interpretation of the references to colour in this figure legend, the reader is referred to the Web version of this article.)

decreased in the Surgicel group at 21 days after implantation compared with those at 7 days after implantation ($p < 0.001$, $p = 0.016$ and $p < 0.001$).

The subsets of M2 macrophages for the four groups at 21 days after implantation were further detected, and the retrieved A549 tumors at 21 days after implantation were used as controls. As shown in Fig. 6A and B, the Surgicel group had the most CLEC7A + M2a macrophages, and the GS group had the least. The tumor group had fewer M2a macrophages than the control and biopaper groups ($p = 0.009$ and 0.005). TNFSF14+ M2b macrophages were expressed in the tumor stroma but negatively expressed in the four groups at 21 days after implantation (Fig. 6A and C). The control and biopaper groups had more SLAM + M2c macrophages than the other groups, and the GS group had the fewest M2c macrophages (Fig. 6A and D). As presented in Fig. 6A and E, VEGF-A was expressed at new microvessels and abundant in the tumor cytoplasm. In terms of tumor control, double F4/80 and VEGF-A+ cells (M2d macrophages) were distributed in tumor nests and the stroma. The M2d macrophage numbers in the GS group were similar to those in the tumor

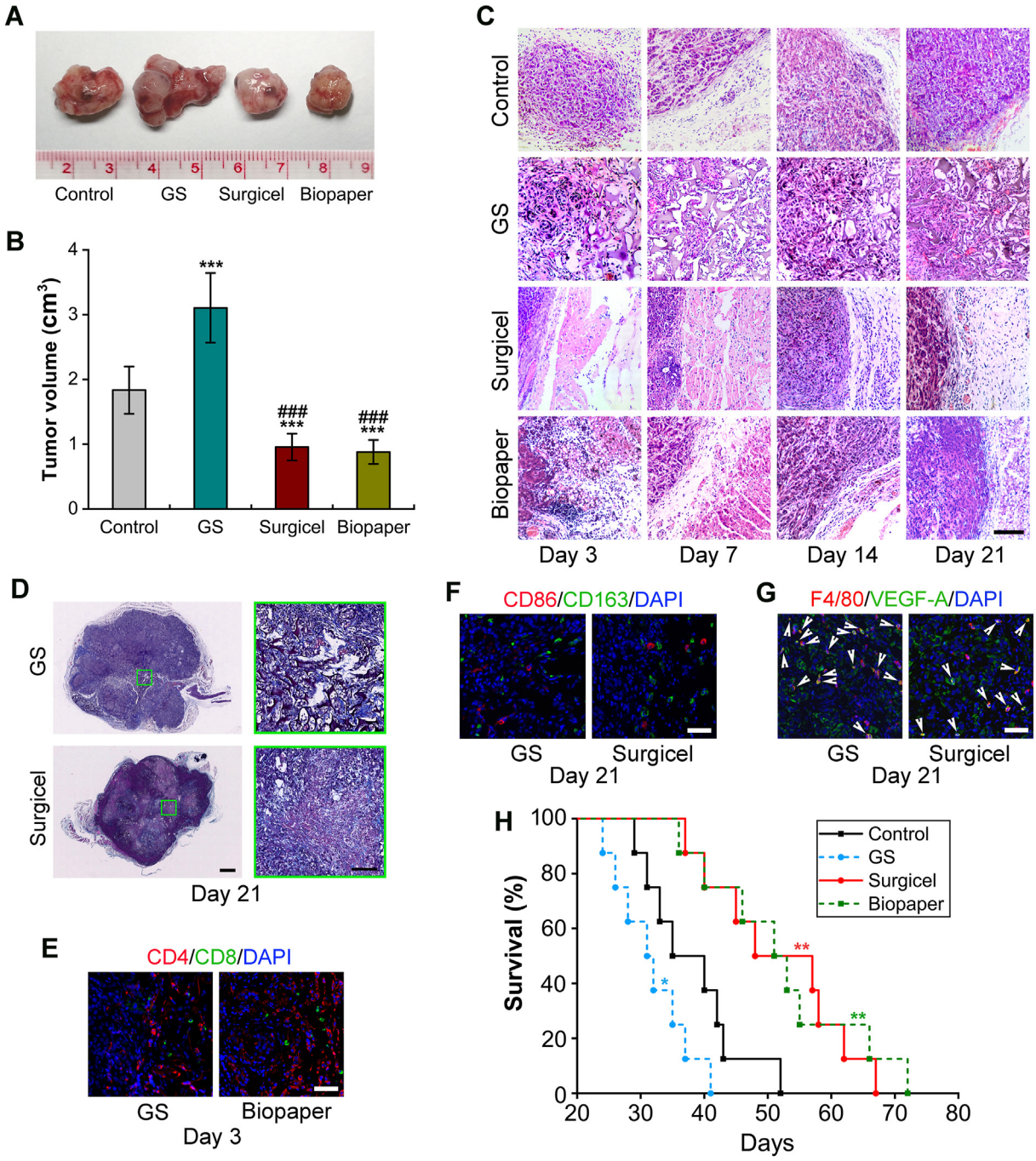

Fig. 7. Subcutaneous implantation of A549 cells with hemostatic materials. (A) Gross examination of subcutaneous tumors at 21-day harvest for the control, GS, Surgicel and biopaper groups. (B) Tumor volume comparison for the four groups at 21-day retrieval. Data are presented as the mean ± SD (***$p < 0.001$ versus the control group; ###$p < 0.001$ versus the GS group). (C) Representative H&E staining for the four groups at 3, 7, 14 and 21-day retrieval (scale bar = 200 μm). (D) Representative Masson's trichrome staining for the GS and Surgicel groups at 21-day retrieval (scale bar = 1 mm and 200 μm for original and amplified images). (E–G) Representative double immunofluorescence staining of $CD4^+$ and $CD8^+$ T cells, $CD86^+$ and CD163+ macrophages, and F4/80+ and VEGF-A + M2d macrophages (scale bar = 50 μm). The arrows show the M2d macrophages. (H) Kaplan–Meier survival curve of the four groups (*$p < 0.05$ and **$p < 0.01$ versus the control group).

group ($p = 0.219$). The other groups had few M2d macrophages. Western blot analysis results are presented in Fig. 6F–J, which showed that the highest expression of CCL1 and CXCL8 proteins were in the tumor tissues, but low expression of CCL1 was observed in the four groups, implying the exclusion of M2b macrophages from the biomaterial-mediated M2 macrophage-like reaction. The GS group had the second highest CXCL8 expression, which was consistent with the immunofluorescence staining results for M2d macrophages. The Surgicel group expressed the highest CLEC7A protein levels, and the biopaper group expressed the highest SLAM protein levels, while the GS group expressed the lowest levels of these two proteins.

3.4. The fastest tumor growth occurred in the gelatin sponge group after subcutaneous implantation of A549 cells and hemostatic materials

Fig. 7A and B shows the gross tumor appearances and the tumor volumes at 21-day retrieval. The GS group had the largest tumor volumes, followed by the control group. The biopaper group and the Surgicel group had comparable tumor volumes ($p = 0.514$). Fig. 7C presents the H&E staining results for the four groups at 3, 7, 14 and 21-day retrieval. For the control group, the tumor cells aggregated to form solid nest-like structures at 3 days after implantation, and the tumor nest range increased with time, with similar nonspecific stromal cell reactions observed at different implantation times. In the GS group, host cells infiltrated into the open space of GS at 3 days after implantation, and tumor cells repopulated the open space of GS at 7 days after implantation. The open space of the GS was abundantly distributed with microvessels at 21 days after implantation. The structure of the GS was obviously damaged at 14 and 21 days after implantation. For the Surgicel group, at 3 days after implantation, the tumor cell nest was in contact with both the thrombosis and the fiber structure of Surgicel. The thrombosis and fiber structure of Surgicel were infiltrated by host cells at 7 days after implantation. At 14 and 21-day retrieval, the Surgicel fiber structures were replaced by host fiber tissues. For the biopaper group at 3 days after implantation, a large number of lymphocytes were distributed in the stroma around the tumor nests. The lymphocyte reaction decreased at 7 days after implantation and disappeared at 14 days after implantation. The stromal structures at 14 and 21 days after implantation were similar to those of the control group. Masson staining in Fig. 7D shows that GS became small, with host cells and A549 cells infiltrating into the open spaces. The structure of Surgicel could not be clearly visualized, with host cells, A549 cells and collagen fiber occupation.

Immunofluorescence staining for subtypes of T cells in Fig. 7E revealed a large number of $CD4^+$ T cells and few $CD8^+$ cells in the GS group, and the biopaper group had more $CD4^+$ T cells and fewer $CD8^+$ cells than the GS group at 3 days after implantation. Immunofluorescence staining for subtypes of macrophages in Fig. 7F shows that the GS group and Surgicel group had a higher proportion of CD163+ macrophages (M2 macrophages) than $CD86^+$ macrophages (M1 macrophages) at 21 days after implantation. F4/80 and VEGF-A double immunofluorescence staining shown in Fig. 7G presented more M2d macrophages infiltrated into the GS group than into the Surgicel group. Fig. 7H shows that the GS group had the shortest OS, and the control group had the second shortest OS. There were no differences in OS between the Surgicel and biopaper groups ($p = 0.835$).

4. Discussion

Commonly used naturally derived hemostatic materials have different ECM structures and components. The tissue source, ECM structure and composition, physical form, chemical crosslinking and terminal sterilization may influence the cellular response of the host [26,32]. Gelatin sponges (GS) in this study were prepared with glutaraldehyde. It has been reported that glutaraldehyde-crosslinked collagen-based biomaterials are toxic to host cells *in vitro* and *in vivo* due to the release of unreacted glutaraldehyde or collagen degradation products [33–35]. In the present study, GS resisted dissolution in the culture medium and presented continuous cytotoxicity to A549 cells, and the GS extract also showed cytotoxicity to A549 cells. The cell numbers of the GS group decreased with time, implying continuous release of toxic substance from GS. As an oxidized regenerated cellulose, Surgicel also presented cytotoxicity [36], and the cytotoxicity was derived from the strongly acidic nature during degradation [37]. Herein, Surgicel did not completely dissolve in the culture medium and presented a little cytotoxicity to A549 cells. The cell number in the Surgicel group was similar to the GS group at 2 days of culture, implying cytotoxicity to A549 cells. But the cell number gradually increased from 4 to 10 days of culture, implying a decrease in cytotoxicity over time. The biopaper dissolved easily in the culture media and generated a gel-like structure, which formed a 3D matrix for tumor cell culture during the first two days, promoting more cell proliferation than 2D culture. As a result, the biopaper group had the highest cell numbers per well at 2 and 4 days of culture compared with the other groups. However, the fast depletion of materials due to culture medium replacement terminated its effect on the proliferation of A549 cells, so the cell numbers in the biopaper group at 6, 8 and 10 days of culture were similar to the control group. These results suggest that biopaper has little toxicity to A549 cells.

Angiogenic growth factors play vital roles in tissue and tumor vascularization, and the levels of expression are regulated by both cell culture conditions and cell-ECM interactions [38,39]. Tumor cells cultured in the biopaper group exhibited more angiogenic growth factor secretion than the other groups, which influenced the cellular behavior of endothelial cells and promoted the vascularization of tissues and tumors. However, the *in vivo* implantation results revealed that tumor growth was decreased in the biopaper group compared with the nonmaterial control group, which was inconsistent with the *in vitro* cell culture results. This can be explained by the host cell reaction *in vivo*. Biopaper is a mixture of sodium hyaluronate and carboxymethyl chitosan. Since the hydrophilicity of sodium hyaluronate, biopaper was dissolved in several minutes and degraded in several days after *in vivo* implantation [40]. The fast dissolution and degradation of the biopaper evoke a vigorous $CD3^+$ T lymphocyte response at the acute phase. These cells were confirmed to be predominantly $CD4^+$ Th1 phenotype T helper cells, which inhibit tumor cell proliferation (Fig. 8). Although the biopaper-induced acute T cell reaction disappeared with time, the tumor volume was decreased, and OS was prolonged.

Oxidized cellulose-based biomaterials showed a faster degradation rate than collagen-based hemostatic materials [41]. As a regenerated oxidized cellulose, the original structures of Surgicel disappeared in this study at 14 and 21-day retrieval, suggesting complete degradation of Surgicel by the host cells. For collagen-based GS, although continuous glutaraldehyde-related toxicity released from GS to host cells and A549 cells, host cells and A549 cells infiltrated into the deep layer of GS, with the formation of host collagen fibers, implying a decrease in glutaraldehyde-related toxicity for *in vivo* GS implantation over time. Fibrosis involves the activation of fibroblasts and deposition of dense collagen components, and GS components were found to be partially degraded with time. T cells, macrophages and their subtypes were detected with immunofluorescence staining, and the results showed an inflammatory reaction mediated by acute and chronic inflammatory cells. GS and Surgicel induced slight acute T lymphocyte responses but marked chronic macrophage inflammatory reactions.

Macrophages around biomaterials have two origins: tissue resident macrophages and monocyte-derived tissue macrophages from the migration of circulating monocytes [42]. In fact, the macrophage properties of the control group reflect those of the resident tissue macrophages. The control group had a larger number of M2 macrophages than M1 macrophages, implying that the main M2 macrophages were resident tissue macrophages. The macrophages infiltrating into the GS and Surgicel showed a balance between M1-like and M2-like phenotypes at acute and chronic phases, and the ratios of M2-like macrophages and Th2 $CD4^+$ T cells increased over time in the GS group. Biologic scaffold

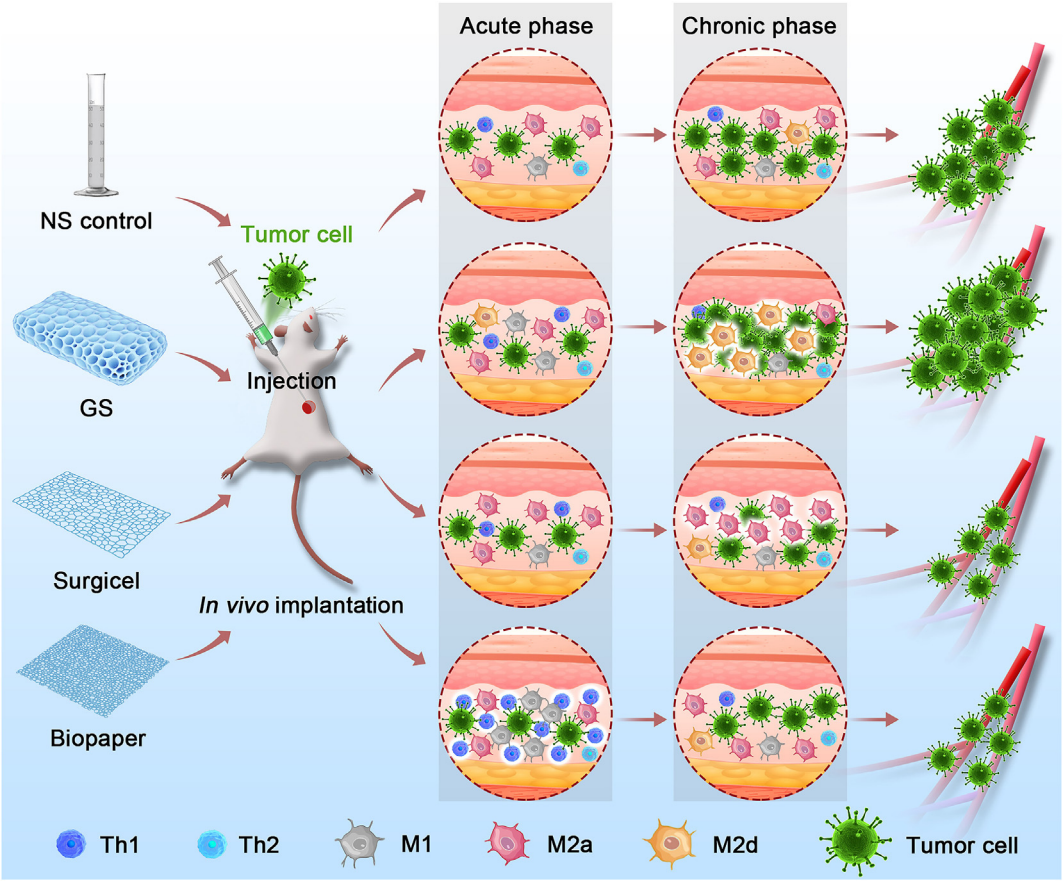

Fig. 8. Schematic illustration of immune cell-hemostatic material interactions on the *in vivo* proliferation of A549 cells.

implantation increased the number and proportion of M2 macrophages at the site of remodeling [43]. Wolf and colleagues revealed that implantation of a urinary bladder matrix (UBM) scaffold created a type 2-like immune response, with an M2 phenotype bias increasing M2-related genes and decreasing M1-related genes [16]. In the present study, the GS group presented an increase in M2/M1 polarization over time, accompanied by an increase in M2 macrophages. The Surgicel group also showed an increase in M2/M1 polarization with time but a decrease in M1-and M2-related proteins, possibly due to the gradual degradation of Surgicel.

The *in vivo* tumor implantation results showed that the GS group had the largest tumor volume and the shortest OS, which was inconsistent with the *in vitro* cell culture results. The inflammatory cells in the GS group and the tumor cell interaction area were hybrid CD4+/CD8+ lymphocytes and M1/M2 macrophages, but the type 2 phenotype was predominant. For the Surgicel group, in the material degradation area, macrophages were the major M2 subtype. This was consistent with the subcutaneous implantation performance of hemostatic materials without tumor cells. The type 1 phenotype has an antitumor effect, but the type 2 phenotype is considered a tumor-associated macrophage (TAM). Higher infiltration of M2 macrophages is related to more aggressive tumor features, including increased tumor progression, invasion, and metastases [44]. However, the results showed a tumor-cytotoxic environment, even an increase in M2 macrophages, in the Surgicel group but a tumor-permissive property in the GS group over time after implantation, which is inconsistent with the increase in malignant behavior of tumors via M2 macrophages.

M2 macrophages consist of four subtypes, named M2a-d, and more subtypes involved in inducing stimuli, metabolic adaptation, surface marker expression, gene expression and related functions [42,44]. M2a and M2c subtypes are involved in tissue fibrosis and tissue remodeling and possess antitumorigenic effects similar to M1 macrophages [45]. M2b and M2d macrophages promote the survival, growth, angiogenesis, invasion, and recurrence of tumors *in vitro* and *in vivo* and are considered the main components of TAMs [46–49]. CCL1 and TNFSF14 are specifically expressed in M2b macrophages [47], so we used these two markers to exclude M2b macrophages. VEGF-A and CXCL8 are highly expressed in M2d macrophages [50], but VEGF-A is also expressed in new vascular endothelial cells. We used F4/80 and VEGF-A double staining to detect M2d macrophages. In the present study, the infiltrated M2-like macrophages in the Surgicel group were confirmed to be predominant M2a subtypes, excluding the M2b and M2d subtypes (Fig. 8). This can explain why the pro-regenerative type 2 phenotype induced by the ECM-based biomaterials did not promote but rather inhibited tumor growth. This finding is interesting because previous studies on macrophage polarization to inhibit tumors focused on M2 to M1 induction. The present study showed that M2a macrophages may also be induced due to their antitumorigenic effects. GS evoked a hybrid M1/M2 macrophage reaction, but M2 macrophages were further confirmed to be the predominant M2d subtype, which promoted tumor growth and lessened OS in the GS group (Fig. 8).

However, there are some issues that need to be addressed. Macrophage polarization is a continuum of functional states depending on their origins and cytokines present in the microenvironment [51]. Macrophages with different subtypes have overlapping markers and functions. For instance, TNF-α is highly expressed in M1 and M2b macrophages [42]. CD86 is used as a marker of M1 macrophages, but it is also expressed on M2b macrophages [52]. M2a and M2c macrophages have similar surface markers, such as CD206, IL-10 and TGF-β. They both attenuate acute and chronic inflammation, promote the Th2 response and induce ECM synthesis [42]. Moreover, whether glutaraldehyde crosslinks or the structures and components of GS lead to the M2d macrophage

reaction needs further study in the future.

5. Conclusions

We demonstrated that three commonly used hemostatic materials, gelatin sponge, Surgicel and biopaper, had different effects on A549 cell growth and proliferation *in vitro* and *in vivo*. The gelatin sponge and Surgicel resisted *in vitro* dissolution and *in vivo* degradation and evoked continuous *in vivo* inflammatory reactions. The gelatin sponge induced a hybrid M1/M2 macrophage reaction, and Surgicel induced an M2 macrophage reaction. Further investigation of infiltrated M2 macrophages showed the presence of an antitumor M2a subset in the Surgicel group but a protumor M2d subset in the gelatin sponge group. Biopaper induced an acute Th1 lymphocyte response at the initial implantation and decreased *in vivo* tumor proliferation. Therefore, Surgicel and biopaper are safe in use for cancer surgery, but gelatin sponges promote *in vivo* tumor growth and are not suitable for tumor bed hemostasis.

Credit author statement

Wei-Dong Lü: Experiments design & synthesis, Project administration, Writing – original draft. Yi-Zhi Liu: Supervision. Yan-Qi Yang: Investigation, Visualization. Kun Zhao: Experiments synthesis, Data Formal analysis. Jian-Rong Lu: Writing – review & editing. Guang-Yan Lei: Software, Validation. Yi-Yu Wang: Investigation. Lin Cai: Visualization. Rui-Fang Sun: Writing- Reviewing & Editing, Funding acquisition.

Declaration of competing interest

The authors declare that they have no known competing financial interests or personal relationships that could have appeared to influence the work reported in this paper.

Acknowledgements

This project is financially supported by the National Natural Science Foundation of China (Project No. 81802788), the Natural Science Foundation of Shaanxi Province of China (Project No. 2018JM7024) and Incubation Project for the National Natural Science Foundation of Tumor Hospital of Shaanxi Province (Project No. SC211708).

Appendix A. Supplementary data

Supplementary data to this article can be found online at https://doi.org/10.1016/j.mtbio.2022.100233.

References

[1] D.A. Hickman, C.L. Pawlowski, U.D.S. Sekhon, J. Marks, A.S. Gupta, Biomaterials and advanced technologies for hemostatic management of Bleeding, Adv. Mater. 30 (4) (2018) 1700859.
[2] F. Signorelli, N. Montano, Use and efficacy of hemostats in neurosurgery, Surg. Technol. Int. 37 (2020) 414–419.
[3] J.J. Li, Y. Yang, Q. Wan, H. Li, Q.M. Long, P.R. Zhang, Clinical observation of the regeneration process of defects after breast cancer resection, BMC Wom. Health 21 (1) (2021) 99.
[4] S. Zhang, J. Li, S. Chen, X. Zhang, J. Ma, J. He, Oxidized cellulose-based hemostatic materials, Carbohydr. Polym. 230 (2020) 115585.
[5] G. Franceschini, G. Visconti, A.M. Sanchez, A. Di Leone, M. Salgarello, R. Masetti, Oxidized regenerated cellulose in breast surgery: experimental model, J. Surg. Res. 198 (1) (2015) 237–244.
[6] H. Wang, P. Chen, Surgicel((R)) (oxidized regenerated cellulose) granuloma mimicking local recurrent gastrointestinal stromal tumor: a case report, Oncol. Lett. 5 (5) (2013) 1497–1500.
[7] M.A. Khan, M. Mujahid, A review on recent advances in chitosan based composite for hemostatic dressings, Int. J. Biol. Macromol. 124 (2019) 138–147.
[8] V. Deineka, O. Sulaieva, N. Pernakov, J. Radwan-Pragłowska, L. Janus, V. Korniienko, Y. Husak, A. Yanovska, I. Liubchak, A. Yusupova, M. Piatkowski, A. Zlatska, M. Pogorielov, Hemostatic performance and biocompatibility of chitosan-based agents in experimental parenchymal bleeding, Mater. Sci. Eng. C Mater. Biol. Appl. 120 (2021) 111740.
[9] C. Zheng, Q. Zeng, S. Pimpi, W. Wu, K. Han, K. Dong, T. Lu, Research status and development potential of composite hemostatic materials, J. Mater. Chem. B 8 (25) (2020) 5395–5410.
[10] Z. Wu, W. Zhou, W. Deng, C. Xu, Y. Cai, X. Wang, Antibacterial and hemostatic thiol-modified chitosan-immobilized AgNPs composite sponges, ACS Appl. Mater. Interfaces 12 (18) (2020) 20307–20320.
[11] W.D. Lu, R.F. Sun, Y.R. Hu, J.R. Lu, L. Gu, Z.G. Liu, G.Y. Lei, Z. Qiang, L. Cai, Photooxidatively crosslinked acellular tumor extracellular matrices as potential tumor engineering scaffolds, Acta Biomater. 71 (2018) 460–473.
[12] J. Li, Y. Zhou, W. Chen, Z. Yuan, B. You, Y. Liu, S. Yang, F. Li, C. Qu, X. Zhang, A novel 3D in vitro tumor model Based on silk fibroin/chitosan scaffolds to mimic the tumor microenvironment, ACS Appl. Mater. Interfaces 10 (43) (2018) 36641–36651.
[13] V. Brancato, J.M. Oliveira, V.M. Correlo, R.L. Reis, S.C. Kundu, Could 3D models of cancer enhance drug screening? Biomaterials 232 (2020) 119744.
[14] S.F. Badylak, T. Hoppo, A. Nieponice, T.W. Gilbert, J.M. Davison, B.A. Jobe, Esophageal preservation in five male patients after endoscopic inner-layer circumferential resection in the setting of superficial cancer: a regenerative medicine approach with a biologic scaffold, Tissue Eng. 17 (11–12) (2011) 1643–1650.
[15] I. Wu, Z. Nahas, K.A. Kimmerling, G.D. Rosson, J.H. Elisseeff, An injectable adipose matrix for soft-tissue reconstruction, Plast. Reconstr. Surg. 129 (6) (2012) 1247–1257.
[16] M.T. Wolf, S. Ganguly, T.L. Wang, C.W. Anderson, K. Sadtler, R. Narain, C. Cherry, A.J. Parrillo, B.V. Park, G. Wang, F. Pan, S. Sukumar, D.M. Pardoll, J.H. Elisseeff, A biologic scaffold-associated type 2 immune microenvironment inhibits tumor formation and synergizes with checkpoint immunotherapy, Sci. Transl. Med. 11 (477) (2019).
[17] P. Shen, Y. Chen, S. Luo, Z. Fan, J. Wang, J. Chang, J. Deng, Applications of biomaterials for immunosuppression in tissue repair and regeneration, Acta Biomater. 126 (2021) 31–44.
[18] Z. Sheikh, P.J. Brooks, O. Barzilay, N. Fine, M. Glogauer, Macrophages, foreign Body giant cells and their response to implantable Biomaterials, Materials 8 (9) (2015) 5671–5701.
[19] R. Klopfleisch, F. Jung, The pathology of the foreign body reaction against biomaterials, J. Biomed. Mater. Res. 105 (3) (2017) 927–940.
[20] F. Taraballi, M. Sushnitha, C. Tsao, G. Bauza, C. Liverani, A. Shi, E. Tasciotti, Biomimetic tissue engineering: tuning the immune and inflammatory response to implantable Biomaterials, Adv. Health. Mater. 7 (17) (2018), e1800490.
[21] D.P. Vasconcelos, A.P. Aguas, M.A. Barbosa, P. Pelegrin, J.N. Barbosa, The inflammasome in host response to biomaterials: bridging inflammation and tissue regeneration, Acta Biomater. 83 (2019) 1–12.
[22] I. Mellman, G. Coukos, G. Dranoff, Cancer immunotherapy comes of age, Nature 480 (7378) (2011) 480–489.
[23] O.A. Haabeth, B. Bogen, A. Corthay, A model for cancer-suppressive inflammation, OncoImmunology 1 (7) (2012) 1146–1155.
[24] D.G. DeNardo, J.B. Barreto, P. Andreu, L. Vasquez, D. Tawfik, N. Kolhatkar, L.M. Coussens, CD4(+) T cells regulate pulmonary metastasis of mammary carcinomas by enhancing protumor properties of macrophages, Cancer Cell 16 (2) (2009) 91–102.
[25] H.A.M. Alsheikh, B.J. Metge, C.M. Ha, D.C. Hinshaw, M.S.V. Mota, S.C. Kammerud, T. Lama-Sherpa, N. Sharafeldin, A.R. Wende, R.S. Samant, L.A. Shevde, Normalizing glucose levels reconfigures the mammary tumor immune and metabolic microenvironment and decreases metastatic seeding, Cancer Lett. 517 (2021) 24–34.
[26] M.C. Cramer, S.F. Badylak, Extracellular matrix-Based Biomaterials and their influence upon cell Behavior, Ann. Biomed. Eng. 48 (7) (2020) 2132–2153.
[27] A.L. Predeina, M.S. Dukhinova, V.V. Vinogradov, Bioreactivity of decellularized animal, plant, and fungal scaffolds: perspectives for medical applications, J. Mater. Chem. B 8 (44) (2020) 10010–10022.
[28] W.D. Lu, M. Zhang, Z.S. Wu, T.H. Hu, Z.J. Xu, W. Liu, Y.R. Hu, The performance of photooxidatively crosslinked acellular bovine jugular vein conduits in the reconstruction of connections between pulmonary arteries and right ventricles, Biomaterials 31 (10) (2010) 2934–2943.
[29] W.D. Lu, L. Zhang, C.L. Wu, Z.G. Liu, G.Y. Lei, J. Liu, W. Gao, Y.R. Hu, Development of an acellular tumor extracellular matrix as a three-dimensional scaffold for tumor engineering, PLoS One 9 (7) (2014), e103672.
[30] W.D. Lu, Y.Z. Liu, Z.G. Liu, C.L. Wu, G.Y. Lei, X. Zhang, W. Gao, Y.R. Hu, Effect of lyophilization technique and gamma-ray sterilization on structural, mechanical and biological properties of acellular tumor extracellular matrix scaffolds, J. Biomater. Tiss. Eng. 6 (3) (2016) 224–231.
[31] R.M. Wang, T.D. Johnson, J. He, Z. Rong, M. Wong, V. Nigam, A. Behfar, Y. Xu, K.L. Christman, Humanized mouse model for assessing the human immune response to xenogeneic and allogeneic decellularized biomaterials, Biomaterials 129 (2017) 98–110.
[32] E. Antmen, N.E. Vrana, V. Hasirci, The role of biomaterials and scaffolds in immune responses in regenerative medicine: macrophage phenotype modulation by biomaterial properties and scaffold architectures, Biomater. Sci. 9 (24) (2021) 8090–8110.
[33] R.A. Manji, L.F. Zhu, N.K. Nijjar, D.C. Rayner, G.S. Korbutt, T.A. Churchill, R.V. Rajotte, A. Koshal, D.B. Ross, Glutaraldehyde-fixed bioprosthetic heart valve conduits calcify and fail from xenograft rejection, Circulation 114 (4) (2006) 318–327.
[34] P. Aguiari, L. Iop, F. Favaretto, C.M. Fidalgo, F. Naso, G. Milan, V. Vindigni, M. Spina, F. Bassetto, A. Bagno, R. Vettor, G. Gerosa, In vitro comparative

assessment of decellularized bovine pericardial patches and commercial bioprosthetic heart valves, Biomed. Mater. 12 (1) (2017), 015021.
[35] K. Adamiak, A. Sionkowska, Current methods of collagen cross-linking: Review, Int. J. Biol. Macromol. 161 (2020) 550–560.
[36] B. Hexig, R. Nakaoka, T. Tsuchiya, Safety evaluation of surgical materials by cytotoxicity testing, J. Artif. Organs 11 (4) (2008) 204–211.
[37] U. Aydemir Sezer, I. Sahin, B. Aru, H. Olmez, G. Yanikkaya Demirel, S. Sezer, Cytotoxicity, bactericidal and hemostatic evaluation of oxidized cellulose microparticles: structure and oxidation degree approach, Carbohydr. Polym. 219 (2019) 87–94.
[38] C. Fischbach, R. Chen, T. Matsumoto, T. Schmelzle, J.S. Brugge, P.J. Polverini, D.J. Mooney, Engineering tumors with 3D scaffolds, Nat. Methods 4 (10) (2007) 855–860.
[39] M. Heller, H.K. Bauer, R. Schwab, S. Blatt, K. Peters, S. Nezi-Cahn, R.E. Unger, A. Hasenburg, W. Brenner, The impact of intercellular communication for the generation of complex multicellular prevascularized tissue equivalents, J. Biomed. Mater. Res. 108 (3) (2020) 734–748.
[40] C.R. Wang, H. Jiang, H.Y. Cao, Q.Q. Huang, Y.P. Song, X.J. Peng, D.D. Chen, Q. Zhang, T.F. Xi, Biocompatibility investigation of haemostatic and anti-adhesive biopaper, Chin. J. Biomed. Eng. 26 (2) (2007) 293–295.
[41] P. Slezak, X. Monforte, J. Ferguson, S. Sutalo, H. Redl, H. Gulle, D. Spazierer, Properties of collagen-based hemostatic patch compared to oxidized cellulose-based patch, J. Mater. Sci. Mater. Med. 29 (6) (2018) 71.
[42] R. Klopfleisch, Macrophage reaction against biomaterials in the mouse model - phenotypes, functions and markers, Acta Biomater. 43 (2016) 3–13.
[43] B.N. Brown, R. Londono, S. Tottey, L. Zhang, K.A. Kukla, M.T. Wolf, K.A. Daly, J.E. Reing, S.F. Badylak, Macrophage phenotype as a predictor of constructive remodeling following the implantation of biologically derived surgical mesh materials, Acta Biomater. 8 (3) (2012) 978–987.
[44] S.S. Sedighzadeh, A.P. Khoshbin, S. Razi, M. Keshavarz-Fathi, N. Rezaei, A narrative review of tumor-associated macrophages in lung cancer: regulation of macrophage polarization and therapeutic implications, Transl. Lung Cancer Res. 10 (4) (2021) 1889–1916.
[45] Y. Li, L. Cai, H. Wang, P. Wu, W. Gu, Y. Chen, H. Hao, K. Tang, P. Yi, M. Liu, S. Miao, D. Ye, Pleiotropic regulation of macrophage polarization and tumorigenesis by formyl peptide receptor-2, Oncogene 30 (36) (2011) 3887–3899.
[46] Q. Wang, H. Ni, L. Lan, X. Wei, R. Xiang, Y. Wang, Fra-1 protooncogene regulates IL-6 expression in macrophages and promotes the generation of M2d macrophages, Cell Res. 20 (6) (2010) 701–712.
[47] L.X. Wang, S.X. Zhang, H.J. Wu, X.L. Rong, J. Guo, M2b macrophage polarization and its roles in diseases, J. Leukoc. Biol. 106 (2) (2019) 345–358.
[48] M.M. Chen, X. Xiao, X.M. Lao, Y. Wei, R.X. Liu, Q.H. Zeng, J.C. Wang, F.Z. Ouyang, D.P. Chen, K.W. Chan, D.C. Shi, L. Zheng, D.M. Kuang, Polarization of tissue-resident TFH-like cells in human hepatoma bridges innate monocyte inflammation and M2b macrophage polarization, Cancer Discov. 6 (10) (2016) 1182–1195.
[49] A. Asai, Y. Tsuchimoto, H. Ohama, S. Fukunishi, Y. Tsuda, M. Kobayashi, K. Higuchi, F. Suzuki, Host antitumor resistance improved by the macrophage polarization in a chimera model of patients with HCC, OncoImmunology 6 (4) (2017), e1299301.
[50] D. Duluc, Y. Delneste, F. Tan, M.P. Moles, L. Grimaud, J. Lenoir, L. Preisser, I. Anegon, L. Catala, N. Ifrah, P. Descamps, E. Gamelin, H. Gascan, M. Hebbar, P. Jeannin, Tumor-associated leukemia inhibitory factor and IL-6 skew monocyte differentiation into tumor-associated macrophage-like cells, Blood 110 (13) (2007) 4319–4330.
[51] M. Lavy, V. Gauttier, N. Poirier, S. Barille-Nion, C. Blanquart, Specialized pro-resolving mediators mitigate cancer-related inflammation: role of tumor-associated macrophages and therapeutic opportunities, Front. Immunol. 12 (2021) 702785.
[52] B. Zhang, W.M. Bailey, K.J. Braun, J.C. Gensel, Age decreases macrophage IL-10 expression: implications for functional recovery and tissue repair in spinal cord injury, Exp. Neurol. 273 (2015) 83–91.